THE JOURNAL OF PHYSICAL CHEMISTRY A

Article

pubs.acs.org/JPCA

Spectroscopy of Cold LiCa Molecules Formed on Helium Nanodroplets

Günter Krois, Johann V. Pototschnig, Florian Lackner,* and Wolfgang E. Ernst*

Institute of Experimental Physics, Graz University of Technology, Petersgasse 16, A-8010 Graz, Austria

ABSTRACT: We report on the formation of mixed alkali−alkaline earth molecules (LiCa) on helium nanodroplets and present a comprehensive experimental and theoretical study of the ground and excited states of LiCa. Resonance enhanced multiphoton ionization time-of-flight (REMPI-TOF) spectroscopy and laser induced fluorescence (LIF) spectroscopy were used for the experimental investigation of LiCa from 15000 to 25500 cm^{-1}. The $4^2\Sigma^+$ and $3^2\Pi$ states show a vibrational structure accompanied by distinct phonon wings, which allows us to determine molecular parameters as well as to study the interaction of the molecule with the helium droplet. Higher excited states ($4^2\Pi$, $5^2\Sigma^+$, $5^2\Pi$, and $6^2\Sigma^+$) are not vibrationally resolved and vibronic transitions start to overlap. The experimental spectrum is well reproduced by high-level ab initio calculations. By using a multireference configuration interaction (MRCI) approach, we calculated the 19 lowest lying potential energy curves (PECs) of the LiCa molecule. On the basis of these calculations, we could identify previously unobserved transitions. Our results demonstrate that the helium droplet isolation approach is a powerful method for the characterization of tailor-made alkali−alkaline earth molecules. In this way, important contributions can be made to the search for optimal pathways toward the creation of ultracold alkali−alkaline earth ground state molecules from the corresponding atomic species. Furthermore, a test for PECs calculated by ab initio methods is provided.

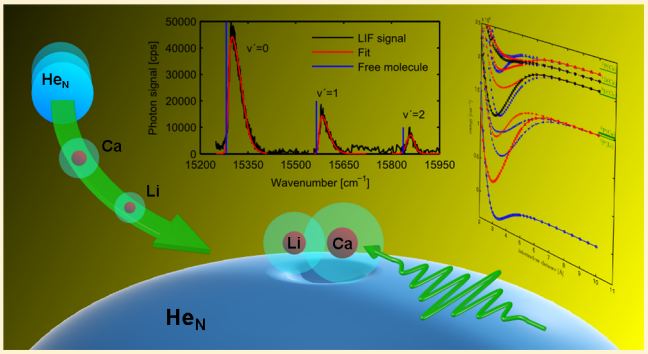

INTRODUCTION

Ultracold polar molecules are attracting considerable attention, and their investigation will extend our knowledge on the physics of ultracold quantum gases into new regimes.[1] A very interesting class of molecules in this regard is represented by mixed alkali−alkaline earth (Ak−Ake) molecules with both electric and magnetic dipole moments in their $^2\Sigma_{1/2}$ electronic ground state. Such molecules are proposed for engineering the lattice spin models of condensed matter physics, a state of matter with topological order, that can be used for the realization of a new class of quantum computation.[2,3] Further applications for ultracold Ak−Ake molecules are precision metrology with the aim to test fundamental physics constants[4,5] or quantum state selective ultracold chemistry.[6]

The most promising starting point for the production of ultracold Ak−Ake molecules are quantum degenerate mixtures of ultracold alkali and alkaline-earth atoms. Though mixtures of homo- and heteronuclear alkali molecules have been studied extensively in the past (see ref 1 and references therein), investigations of Ak−Ake like mixtures have only been reported for LiYb[7−9] and RbYb.[7,10] Recent progress in ultracold atomic physics (e.g. the Bose−Einstein condensation of alkaline earth metal atoms Ca[11] and Sr)[12−14] suggests that the formation of ultracold ground state Ak−Ake molecules is within reach,[15−18] and quantum degenerate mixtures of Rb and Sr atoms have been successfully realized very recently.[19] The standard methods to overcome the gap between the interatomic pair distance in an ultracold atomic gas and the final binding length of the diatomic molecule are to convert ultracold atoms to molecules by either photoassociation[20] or magneto-association[21] followed by coherent population transfer to produce ground state molecules. This approach has been successfully used for the preparation of ground state Cs_2,[22,23] KRb,[24] and Sr_2[25] molecules by stimulated Raman adiabatic passage (STIRAP).

An important requirement for the formation of ultracold molecules is the knowledge of their electronic structure, which is crucial for the search for optimal pathways to couple two colliding atoms with their molecular ground state. Hence the theoretical as well as the experimental exploration of excited states can greatly simplify the navigation through complex molecular potentials and can be used for the prediction of transition frequencies and transition probabilities.

The preparation of Ak−Ake molecules in molecular beams or heat-pipe ovens is complicated, and despite the rising interest in these molecules, only a few spectroscopic data are available. Here we report on a new method for the production of Ak−Ake molecules. Our approach uses helium nanodroplets for the

Special Issue: Terry A. Miller Festschrift

Received: August 5, 2013
Revised: September 11, 2013
Published: September 12, 2013

   dx.doi.org/10.1021/jp407818k | J. Phys. Chem. A 2013, 117, 13719−13731

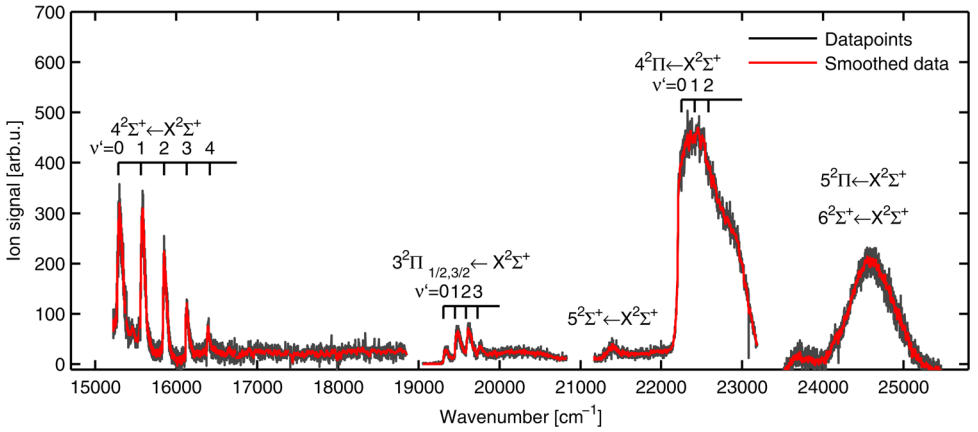

Figure 1. Excitation spectrum of LiCa on He_N as recorded by REMPI-TOF spectroscopy from 15200 to 25500 cm^{-1}. Four band systems have been assigned to the $4^2\Sigma^+ \leftarrow X^2\Sigma^+$, $3^2\Pi_{1/2,3/2} \leftarrow X^2\Sigma^+$, $5^2\Sigma^+ \leftarrow X^2\Sigma^+$, and $4^2\Pi \leftarrow X^2\Sigma^+$ transitions of LiCa on He_N and the peak at 24500 cm^{-1} is assigned to the two overlapping $6^2\Sigma^+ \leftarrow X^2\Sigma^+$ and $5^2\Pi \leftarrow X^2\Sigma^+$ transitions. Molecular beam spectroscopy results[37] are indicated by vibrational scales where available.

isolation of cold (0.37 K) Ak−Ake molecules in their vibronic ground state in a sequential pickup scheme. In the past 20 years, superfluid helium nanodroplets have been established as a matrix for the preparation of tailored molecules.[26] The method of helium nanodroplet isolation spectroscopy has been used previously for the investigation of a class of molecules very similar to Ak−Ake molecules, heteronuclear alkali dimers[27−30] (and also trimers[31−34]) on the surface of helium nanodroplets. The interaction between the molecule and helium droplet, which manifests itself typically in an asymmetric broadening of vibronic transitions, is relatively small and allows the extraction of molecular parameters of free molecules.[35] Furthermore, the structure of the broadened vibronic transition in the recorded spectrum gives insights into the interaction between molecule and helium droplet.[28,36]

We demonstrate our approach on the example of LiCa, a molecule where experimental[37−39] data as well as calculations[16−18,40−42] are available, which allows a detailed comparison with our results. Besides LiBa,[43−45] LiCa is the only system where high resolution spectroscopic data have been obtained.

In addition to the experiment, we present quantum chemical ab initio calculations of the LiCa molecule. The majority of available calculations is focused on the ground state[16−18,41] because of the outstanding properties and the importance for possible applications of ultracold ground state Ak−Ake molecules. Gopakumar et al. have recently presented calculations of the lowest two excited states.[42] The most extensive calculations of LiCa potential energy curves, including higher states, have been presented by Allouche et al.[40] and Russon et al.,[37] which can be compared to our results. Our calculations extend the previous works to higher excited states.

The advantage of our approach compared to previous experiments is that the combination of all Ak and Ake molecules is possible on the droplet with the same experimental arrangement and requires no additional experimental effort. One of the greatest problems in experiments with heat-pipe oven sources[38,39] is the large singlet dimer background of the alkali partner of the Ak−Ake molecule. This disadvantage is overcome by helium nanodroplet isolation spectroscopy, which provides a powerful method for the investigation of vibronic transitions of mixed Ak−Ake molecules.

This manuscript is organized as follows: upon a brief description of the experimental setup and methods we discuss the experimental results. We present the recorded spectra according to their energetic ordering, starting with the $4^2\Sigma^+ \leftarrow X^2\Sigma^+$ transition. For this transition, results from LIF and REMPI spectroscopy are compared. Dispersed emission spectra allow us to draw conclusions on the electronic ground state of LiCa. Subsequently the $3^2\Pi_{1/2,3/2} \leftarrow X^2\Sigma^+$ transition is discussed where isotope shifts and the spin−orbit splitting could be studied. Experimental spectra of higher states are the subject of next section. Furthermore, we compare our theoretical results to experimental spectra. Our findings are summarized in a concluding section.

EXPERIMENTAL SECTION

The experimental setup is described in detail in refs 31 and 46, and a closer description of the resonance enhanced multiphoton ionization time-of-flight detection can be found in ref 47. To give a short overview: The helium droplets are formed by a supersonic jet expansion; i.e., precooled helium gas (T_0 = 15 K) is expanded through a nozzle (d_0 = 5 μm) under high pressure (p_0 = 60 bar) into the vacuum. The produced droplet sizes obey a log-normal distribution,[48] and the given source conditions lead to a droplet size distribution maximum of $\hat{N}_{60,15}$ = 6000, which corresponds to a radius of $\hat{R}_{60,15}$ = 40 Å (assuming spherical droplets[49]). The helium droplet beam is then guided into the pickup chamber where it successively passes through two pickup cells holding small amounts of the corresponding doping elements Li and Ca. Changing the cell temperature affects the probability of each droplet to pick up one or more atoms. The optimum temperatures for the formation of LiCa are T_{Li} = 350 °C and T_{Ca} = 370 °C.

The excitation spectra were recorded using resonance enhanced multiphoton ionization time-of-flight (REMPI-TOF) spectroscopy. In this method the LiCa on the He droplet is excited by a tunable pulsed dye laser (Lambda Physik FL 3002) and ionized by a fraction of the pump laser power (Radiant Dyes RD-EXC 200 XeCl laser, 26 ns pulse duration, 100 Hz) for spectra below 19000 cm^{-1} or by a second photon of the dye laser for spectra above 19000 cm^{-1}. The ion yield is recorded by a time-of-flight mass spectrometer (Jordan D-850 AREF) with angular reflectron.

In addition, the lowest recorded LiCa transition ($4^2\Sigma^+ \leftarrow X^2\Sigma^+$) was investigated by laser induced fluorescence (LIF) spectroscopy. Fluorescent light either was monitored with a

dx.doi.org/10.1021/jp407818k | J. Phys. Chem. A 2013, 117, 13719−13731

Peltier cooled photomultiplier tube (Hamamatsu R943−01) or, for dispersed fluorescence emission spectroscopy, was sent through a modified McPherson EU-700 grating monochromator with an attached CCD camera (LOT-Andor iDUS DU401ABR-DD).

RESULTS AND DISCUSSION

Experimental Results. The excitation spectrum of LiCa on He_N, shown in Figure 1, was recorded with REMPI-TOF spectroscopy in the range 15200−25500 cm^{-1}. The two lowest recorded band systems (the $4^2\Sigma^+ \leftarrow X^2\Sigma^+$ and $3^2\Pi_{1/2,3/2} \leftarrow X^2\Sigma^+$ transitions) consist of a progression of vibrational bands with a characteristic asymmetric (lambda-shaped) peak form. For transitions into higher states the vibrational spacing could not be resolved and the bands appear as broadly extended, structureless features in the spectrum. As the density of states increases, the vibrational bands start to overlap and the complexity of the spectra increases. For three transitions, experimental data from molecular beam spectroscopy experiments are available and can be compared to our results.[37] This allows us to draw conclusions on the interaction between the LiCa molecule and the droplet and the perturbation of molecular states by the droplet. In the following we discuss the recorded transitions in detail, followed by a presentation of calculated potential energy curves and transition dipole moments for LiCa as well as a comparison of calculations and experiments which allows the assignment of the higher excited states.

$4^2\Sigma^+ \rightarrow X^2\Sigma^+$ Transition. The R2PI excitation spectrum of the $^7Li^{40}Ca$ $4^2\Sigma^+ \leftarrow X^2\Sigma^+$ transition is shown in Figure 1 in the range 15200−16300 cm^{-1}. This excited LiCa molecular state correlates to the Li $2s^{1,2}S$ + Ca $4s^13d^1,^3D$ atomic asymptote. The vibrational levels could be resolved and can be followed from $\nu' = 0$−4. The absence of hot bands reveals that in the presence of the low-temperature He_N environment the LiCa molecules are cooled efficiently to the lowest vibrational level $\nu'' = 0$. Hence, upon doping with Li and subsequently with Ca, the molecule is formed in the vibronic ground state $X^2\Sigma^+(\nu''=0)$ and the gained bond formation energy is released into the droplet. The efficient formation of LiCa demonstrates that the two surface bound species, Li^{50} and Ca,[51,52] find each other on the droplet surface and a large fraction does not desorb despite the released binding energy of 2605.3(100) cm^{-1}.[39] The excess energy is carried away by evaporated He atoms, causing a droplet shrinking of about 520 He atoms, if 5 cm^{-1} binding energy of a He atom to the droplet is assumed.[26] The LiCa molecule is more strongly bound than the alkali triplet molecules, but weaker than, for example, the sodium singlet dimers (5942.6880(49) cm^{-1} [53]), which have been investigated on the helium droplet surface extensively.[28] The observed peak structure is characteristic for surface located molecules[28,36,54,55] with strongly coupled vibrational motion to the surface of the helium droplet. Because of the similarities between Li− and Ca−helium interaction energies and the similarities between the spectra of surface bound alkali triplet molecules and the LiCa spectra we expect the LiCa molecule to reside on the surface of the helium droplet.

To increase the signal-to-noise ratio and to avoid saturation effects, we investigated the $4^2\Sigma^+ \leftarrow X^2\Sigma^+$ transition additionally with LIF spectroscopy. Saturation effects can occur due to the relatively high pulse energy of the pulsed dye lasers, which is needed for a reasonable R2PI signal of the molecule on the helium droplet. The LIF excitation spectrum is shown in Figure 2 and was recorded with a continuous wave (cw) ring dye laser operated with DCM (∼500 mW). With LIF spectroscopy only

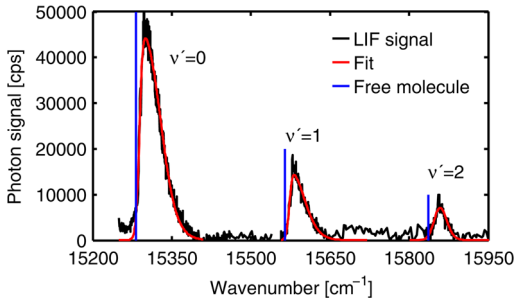

Figure 2. Excitation spectrum of the LiCa $4^2\Sigma^+(\nu'=0-2) \leftarrow X^2\Sigma^+(\nu''=0)$ transition. The signal was fitted with the asymmetric 2σ function given in eq 1. The data have been offset corrected, and the red line has been smoothed. The blue lines denote the free molecule transitions as found in ref 37.

the lowest three vibrational states could be recorded. The LIF spectrum can be compared with the spectrum in Figure 1 in ref 37. The intensities of the $\nu' = 0$ and $\nu' = 1$ peaks in Figure 2 match the relative intensities in ref 37, which demonstrates that the Franck−Condon factors (FCF) are not influenced by the interaction with the droplet for this transition. The vibrational levels obtained for the $4^2\Sigma^+$ state can be compared to spectroscopic data of free LiCa molecules.[37,39] Band origins for the free molecule are shown as vertical blue lines in Figure 2. It can be seen that the onset of the rising edge of the lambda-shaped peaks coincides with the free molecule value. The vibrational bands are broadened and shifted to the blue. The broad "phonon-wing" is caused by the interaction of the excited molecule with the helium droplet. The peaks have a fwhm of 30−40 cm^{-1} and no zero-phonon line could be observed. The peak structure is very similar to the shape of alkali triplet transitions with resolved vibrational levels.[28,35,56] Also the bandwidths compare to alkali triplet transitions (e.g., for the Na_2 $1\Sigma_g^+ \leftarrow 1^3\Sigma_u^+ \sim 30$ cm^{-1} was reported[28]). For the case of alkali triplet molecules[28,36,54,55] it was concluded that a phonon-wing without zero-phonon lines suggests a strong coupling of the vibrational motion of the molecule to the surface of the helium droplet. Hence we conclude that the LiCa molecule is also strongly coupled to the helium droplet.

The peaks in the LIF spectrum were fitted with an asymmetric 2σ-function:[35,57]

$$L(\bar{\nu}) = I(1 + e^{(\bar{\nu}-\bar{\nu}_0+w_1/2)/w_2})^{-1} \times [1 - (1 + e^{(\bar{\nu}-\bar{\nu}_0-w_1/2)/w_3})^{-1}] \quad (1)$$

The maximum of the second derivative of the fit function corresponds to the onset of the rising edge of the peak and hence to the origin of the vibrational band. As has been shown in ref 35 for lithium triplet molecules on helium droplets, this procedure can be used to determine molecular parameters of free molecules and the values for the origins of the vibrational bands agree within a few cm^{-1}. In Table 1 we compare the experimentally determined vibrational band origins from refs 37 and 39 with our fit results. We include the values obtained from the R2PI spectra for the 3−0 and the 4−0 band origins because they agree well with the literature values, indicating that they are not influenced by saturation effects. As shown in Table 1, the results from helium droplet isolation spectroscopy agree very well with the molecular beam[37] and heat-pipe oven[39]

dx.doi.org/10.1021/jp407818k | J. Phys. Chem. A 2013, 117, 13719−13731

Table 1. Vibrational Bands and Molecular Parameters of $^{7}Li^{40}Ca$ for the $4^2\Sigma^+ \leftarrow X^2\Sigma^+$ Transition[a]

	energy (cm^{-1})		
band $\nu'-\nu''$	this work	Russon et al.[37]	Stein et al.[39]
0−0	15282(1)[b]	15282.2	15282.2
1−0	15569(3)[b]	15565.7	15562.8
2−0	15840(3)[b]		15836.7
3−0	16112(2)[c]		16104.3
4−0	16374(1)[c]		16366.3
T_e	15241(15)	15237.6	15240.06
ω_e	288(14)	283.5	287.84
$x_e\omega_e$	3.2(2.8)	3.57	3.86

[a]One standard deviation uncertainties are given in parentheses. [b]Values obtained from LIF spectroscopy. [c]Values obtained from R2PI spectroscopy.

experiments, demonstrating the suitability of our method for the determination of molecular parameters and for testing calculated potential energy curves of free Ak−Ake molecules. The molecular parameters T_e, ω_e, and $x_e\omega_e$ have been calculated from a least-squares fit to the standard expression given in eq 2.[58]

$$T(\nu') = T + \omega_e\left(\nu' + \frac{1}{2}\right) - x_e\omega_e\left(\nu' + \frac{1}{2}\right)^2 \quad (2)$$

Figure 3 shows the $4^2\Sigma^+ \rightarrow X^2\Sigma^+$ emission of LiCa molecules upon excitation of the $4^2\Sigma^+$ $\nu' = 1$, 2, and 3 vibrational levels at

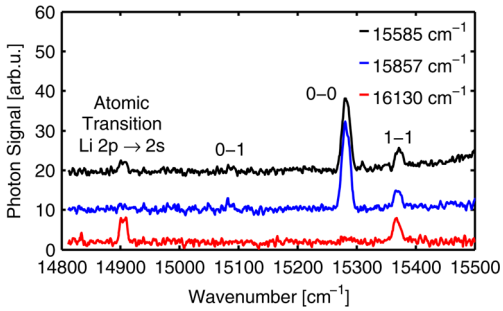

Figure 3. Spectra of the $4^2\Sigma^+ \rightarrow X^2\Sigma^+$ emission of LiCa molecules formed on helium nanodroplets. Emission was collected upon excitation of $\nu' = 1$, 2, and 3 in the $4^2\Sigma^+$ state, which is shown as black, blue, and red lines, respectively. Four peaks corresponding to the molecular 0−1, 0−0, and 1−1 transitions and the Li 2p → 2s transition can be seen in the spectra.

15585, 15857, and 16130 cm^{-1}, respectively. The cw laser was tuned to the phonon-wing maximum of each transition on the helium droplet. Four peaks corresponding to the molecular 0−1, 0−0, and 1−1 transitions and the Li 2p → 2s transition can be seen in the spectra. The observed fluorescence light in the spectrum originates only from free molecules that leave the droplet upon laser excitation. Fluorescence light could only be detected from the lowest two vibrational levels, indicating a droplet mediated cooling of the LiCa molecules in the excited states prior to the emission. Similar results have been reported for the emission spectra after the excitation of alkali dimers.[28,59] The observation of the Li 2p → 2s emission indicates that a considerable fraction of the molecules fragments into Ca and excited Li atoms. Note that excited Ca atoms could not be detected in this experiment because, in this energy range, only the lowest metastable triplet P states can be populated upon fragmentation. Their long lifetime (e.g., ∼4.2 μs for the Ca $^3P_1$ state,[60] the upper state of the strongest intercombination line) forbids a detection in our experiment. A comparison of the three recorded spectra shows that the two signals recorded upon excitation of the $\nu' = 1$ and $\nu' = 2$ levels do not differ strongly, except for an increased Li atomic emission at the former. As can be seen from the spectra, the majority of molecules from which fluorescence light could be detected, are in the vibrational ground state $\nu' = 0$. We conclude that the cold helium environment induces a relaxation of the molecules before they leave the droplet. This demonstrates that the cooling mechanism is very efficient in this case. The striking difference at the excitation of $\nu' = 3$ is the absence of transitions originating from $\nu' = 0$ (i.e., the 0−0 and 0−1 line) accompanied with an increased Li atomic emission. This suggests that in this case for the two competing underlying processes, relaxation and desorption, the latter is faster and prevails. The observation of an increased Li atom signal from the D lines is unexpected because predissociation of the $4^2\Sigma^+$ state upon interaction with the crossing $1^4\Sigma^+$ state was reported to occur above $\nu' = 9$.[39] We think that this observation is related to the interaction between molecule and helium droplet, where due to the presence of the droplet it could also be possible that the $1^2\Delta$ state affects the dynamics of the excited molecule. Our recorded emission spectra demonstrate that the helium droplet isolation technique can be used for the preparation and investigation of free molecules that have desorbed from the droplets upon excitation. Most importantly, the recorded emission spectra give insight into the vibrational levels of the electronic ground state. We think that in further experiments these free molecules can be investigated upon formation on the droplet with additional lasers, allowing spectroscopy of cold tailored molecules without restricted resolution due to the interaction with the droplet.

$3^2\Pi_{1/2,3/2} \rightarrow X^2\Sigma^+$ Transition. Figure 4 shows a detailed view of the $3^2\Pi_{1/2,3/2} \leftarrow X^2\Sigma^+$ transition of LiCa on He_N. The $3^2\Pi$ excited molecular state adiabatically correlates to the same separated atom limit as the $4^2\Sigma^+$ state discussed above (Li $2s^1,^2S$ + Ca $4s^13d^1,^3D$). The data have been fitted with eq 1, and the band origins of the vibrational bands correspond to the free molecule transitions and have been obtained by calculating the maximum of the second derivative of the fit. The fwhm of the peaks is in the range of 80 cm^{-1}. In Table 2 we compare our results with those of a molecular beam experiment,[37] which are, to our knowledge, the only existing experimental data for this transition. The vibrational spacing as obtained by the fits is within several cm^{-1} of the literature values. Please note that the values for the vibronic transitions are compared to the $3^2\Pi_{1/2}$ molecular data, which follows from the fit. The molecular constants have been obtained by a least-squares fit to the standard expression,[58] eq 2. In this case the parameter $x_e\omega_e$ was set to zero, because an inclusion of this parameter resulted in large uncertainties of the molecular parameters. The free molecule values for the parameters T_e and ω_e were calculated from the values given in Table 2 in ref 37. As can be seen from Table 2, the determined parameters lie well within the one σ standard deviation interval and differ only a few cm^{-1} from the free molecule values. The relative intensities of the peaks do not allow us to draw conclusions about the Franck−Condon factors in this case, because the signal has not been normalized with the relative laser pulse energy over the wavelength range.

To highlight the effects that can be seen in the recorded signal, Figure 4 has been divided into three sections. Plot a

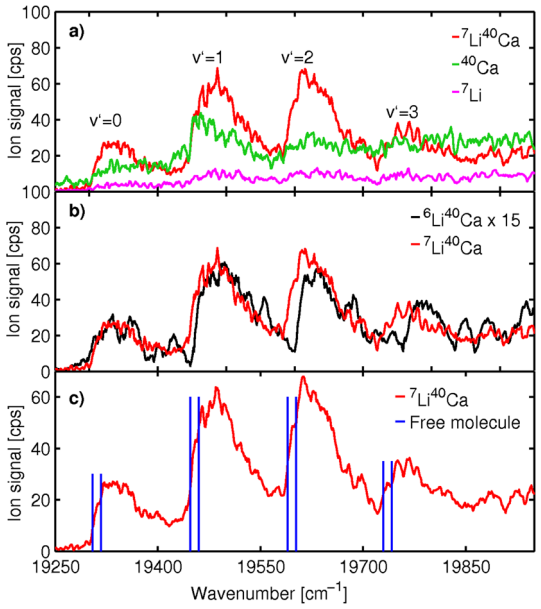

Figure 4. Close-up of the REMPI-TOF signal of the $3^2\Pi_{1/2,3/2} \leftarrow X^2\Sigma^+$ transition. Plot a shows a comparison of the atomic ^{7}Li and ^{40}Ca ion signals to the molecular $^7Li^{40}Ca$ ion signal. Plot b shows the signal for the different isotopologues of LiCa, $^7Li^{40}Ca$ and $^6Li^{40}Ca$, where the latter signal has been scaled by a factor of 15 because of the low abundance of the ^{6}Li isotope. In plot c the effect of spin−orbit splitting can be seen in the form of a slight kink in the rising edge of each peak, which is situated between the corresponding spin−orbit split $^2\Pi$ components of the free molecule transitions, indicated by vertical blue lines.

Table 2. Vibrational Bands for the $3^2\Pi_{1/2} \leftarrow X^2\Sigma^+$ Transition of $^7Li^{40}Ca$ and $^6Li^{40}Ca$ and Molecular Parameters for the $3^2\Pi_{1/2}$ State of Both Isotopologues[a]

	energy (cm^{-1})			
	$^7Li^{40}Ca$		$^6Li^{40}Ca$	
band $\nu'-\nu''$	this work	Russon et al.[37]	this work	Russon et al.[37]
0−0	19302(2)	19304.6	19295(2)	19302.9
1−0	19436(2)	19447.8	19449(3)	19456.0
2−0	19581(1)	19589.6	19600(6)	19607.0
3−0	19721(2)	19729.3	19757(1)	19757.3
T_e	19330(15)	19330.6[b]	19325(8)	19330.6[b]
ω_e	140.2(6.6)	144.5	153.7(3.6)	154.2[b]

[a]One standard deviation uncertainties are given in parentheses. [b]Calculated from values given in Table 2 in ref 37.

shows a comparison of the atomic Li and Ca ion signal to the LiCa molecular ion signal. Atomic calcium follows the trend of LiCa, whereas the atomic Li signal shows only a very weak structure. The $3^2\Pi$ potential energy curve is crossed by the $1^4\Sigma^+$ curve, which gives rise to a predissociation of the LiCa molecule, as has been suggested in refs 37−39. The $1^4\Sigma^+$ curve is purely repulsive above the lowest vibrational level of the $3^2\Pi$ state (case c$^-$ according to Mulliken's classification of predissociation cases[61,62]), leading to ground state Li atoms and Ca atoms excited into their $4s^14p^1$,^{3}P state in the separated atom limit. As suggested in ref 39, the predissociation rate seems to be relatively high. We attribute the observation of the large Ca ion signal that follows the LiCa ion signal to predissociated molecules. However, helium droplets are known to induce relaxation processes, which have been observed in the form of intersystem crossings in alkali triplet dimers[28] and quartet trimers[63] or spin relaxation in atoms doped to helium droplets.[64,65] The LiCa molecules will interact with the helium droplets during the predissociation which can lead to atomic fragments in states different from the dissociation products associated with the $1^4\Sigma^+$ molecular state. Hence predissociation of the LiCa molecule on a helium droplet can give rise to both excited Ca and Li fragments. A contribution of ground state Li atoms to the Li^+ signal is unlikely, because we do not observe a background signal caused by the free atom beam, which is always present in our detection chamber due to our pickup design. In light of this discussion we think that the following effects are responsible for the signals in Figure 4a: The majority of molecules is ionized in a two-photon ionization process and form a stable molecular LiCa ion. A fraction of molecules predissociates, resulting in a Ca ion signal and also a weak Li ion signal caused by the interaction with the droplet. In both cases, for the excited Li and Ca, two photons are necessary for the ionization. A competing process is the fragmentation of the molecule upon absorption of a third photon, which will also contribute to both the Li and the Ca ion signal.

At the $3^2\Pi \leftarrow X^2\Sigma^+$ LiCa transition we were able to separate the signals of $^6Li^{40}Ca$ and $^7Li^{40}Ca$ and thus obtain a spectrum for both isotopologues, which is shown in Figure 4b. Despite the very weak $^6Li^{40}Ca$ signal, due to the low abundance of ^{6}Li (7.4%), the isotope shift can be clearly seen and the trend of an increasing shift for higher excited vibrational levels is obvious. The isotope shift is well comparable to the values given in ref 37, as shown in Table 2. Also the molecular parameters T_e and ω_e for both isotopologues are in good accordance with the literature values.

As has been shown in ref 37, the $3^2\Pi$ state has a fairly large spin−orbit (SO) constant and Hund's case (a) is appropriate for the description of the coupling of spin and orbital angular momentum with the molecular axis. The $3^2\Pi$ state splits into two spin−orbit sub-bands. Due to the broadening of the lines by the interaction with the He droplet, they are hard to resolve. Despite this, in our data a small effect of the spin−orbit splitting (SO constant A'_0 = 13.3 cm^{-1}, for ν' = 0[37]) can be seen in the form of a slight kink in the rising edge of each vibrational band in the $^7Li^{40}Ca$ spectrum. This effect is highlighted in the Figure 4c, where the kink can be seen for each vibrational level ν' = 0−3 between the band origins of the two spin−orbit split $^2\Pi$ components of the free molecule, indicated by the vertical blue lines. It is remarkable that the value of the spin−orbit constant seems to be conserved despite the presence of the droplet. Assuming the molecule lies flat on the surface of the droplet, the symmetry of the system will be reduced and an effect on the SO constant would be expected.[30] However, the coupling of spin and orbital angular momentum to the intermolecular axis seems to be much stronger than the influence of the droplet which would make the effect very small. If on the other hand the molecular axis of the LiCa molecule was aligned perpendicular to the droplet surface, the symmetry around the internuclear axis would also be conserved. This would be another explanation for the observed SO splitting.

Higher Excited States. In this section the single structures that can be seen in Figure 1 in the energy region above 21250 cm^{-1} are discussed. The band at 22000 cm^{-1} has been assigned to the $4^2\Pi \leftarrow X^2\Sigma^+$ transition, where the upper level adiabatically correlates to Li $2s^1$,^{2}S + Ca $4s^13d^1$,^{1}D in the separated atom limit. The transition extends from 22150 to 23100 cm^{-1} and shows a steep rising edge and a high signal on

dx.doi.org/10.1021/jp407818k | J. Phys. Chem. A 2013, 117, 13719−13731

Table 3. Comparison to Theoretically Determined Molecular Parameters of the Ground and Excited States of LiCa

state	property	this work	CASPT2[42]	QCISD(T)[37]	MRCI[37]	CIPSI[40]
$X^2\Sigma^+$	R_e (Å)	3.342	3.400	3.410	3.400	3.296
	ω_e (cm^{-1})	202.6	191	194	204	195.28
	D_e (cm^{-1})	2883	2130.92	2178	2178	2355
$1^2\Pi$	R_e (Å)	2.948	2.985	3.015	3.052	2.862
	ω_e (cm^{-1})	283.5	306	280	286	306.34
	T_e (cm^{-1})	5147	5882.05	6355	6028	5464
	D_e (cm^{-1})	12630	11224.81			
$2^2\Sigma^+$	R_e (Å)	3.503	3.562		3.634	3.423
	ω_e (cm^{-1})	201.7	196		192	219.6
	T_e (cm^{-1})	9461	9702.61		9138	9554
	D_e (cm^{-1})	8360	7279.96			
$2^2\Pi$	R_e (Å)	3.127	3.199		3.346	2.99
	ω_e (cm^{-1})	257	240		206	275.41
	T_e (cm^{-1})	11990	13479.71		13825	12016
	D_e (cm^{-1})	5771	3759.35			
$3^2\Sigma^+$	R_e (Å)	3.199	3.670		3.774	
	ω_e (cm^{-1})	171	164		171	
	T_e (cm^{-1})	12793	13745.06		13704	
	D_e (cm^{-1})	4999	3572.23			
$1^4\Pi$	R_e (Å)	3.221	3.318	3.361	3.394	3.105
	ω_e (cm^{-1})	223	208	201	201	242.19
	T_e (cm^{-1})	13050	13603.72	12390	12815	13169
	D_e (cm^{-1})	4704	3721.44			
$1^2\Delta$	R_e (Å)	3.074				2.968
	ω_e (cm^{-1})	257				275.73
	T_e (cm^{-1})	15036				14754
	D_e (cm^{-1})	8502				
$4^2\Sigma^+$	R_e (Å)	3.398			3.365	3.31
	ω_e (cm^{-1})	270			242	290.46
	T_e (cm^{-1})	15277			19505	14708
	D_e (cm^{-1})	8274				
$1^4\Sigma^+$	R_e (Å)	4.325	5.008	5.600	4.708	
	ω_e (cm^{-1})	67	29.60 ($^6Li^{40}Ca$)			
	T_e (cm^{-1})	17144	17227.63	15505	15915	
	D_e (cm^{-1})	608	265.36			
$1^4\Sigma^-$	R_e (Å)	2.74		2.851	2.925	2.636
	ω_e (cm^{-1})	270		288	286	317.17
	T_e (cm^{-1})	18306		18426	19196	18546
$3^2\Pi$	R_e (A)	3.486			3.507	3.456
	ω_e (cm^{-1})	152			169	149.48
	T_e (cm^{-1})	19444			22545	19122
	D_e (cm^{-1})	4119				
$2^4\Pi$	R_e (Å)	3.793			3.871	
	ω_e (cm^{-1})	159			174	
	T_e (cm^{-1})	20817			22810	
	D_e (cm^{-1})	2720				
$2^4\Sigma^+$	R_e (Å)	3.792				
	ω_e (cm^{-1})	137				
	T_e (cm^{-1})	21397				
	D_e (cm^{-1})	2135				
$5^2\Sigma^+$	R_e (Å)	3.261				
	ω_e (cm^{-1})	236				
	T_e (cm^{-1})	21596				
	D_e (cm^{-1})	3218				
$4^2\Pi$	R_e (Å)	3.432			3.41	
	ω_e (cm^{-1})	179			148	
	T_e (cm^{-1})	21980			23693	
	D_e (cm^{-1})	2837				
$1^4\Delta$	R_e (Å)	4.129				
	ω_e (cm^{-1})	81				
	T_e (cm^{-1})	22841				

Table 3. continued

state	property	this work	CASPT2[42]	QCISD(T)[37]	MRCI[37]	CIPSI[40]
	D_e (cm^{-1})	683				
$2^2\Delta$	R_e (Å)	3.895				
	ω_e (cm^{-1})	101				
	T_e (cm^{-1})	23616				
	D_e (cm^{-1})	1198				
$5^2\Pi$	R_e (Å)	4.204				
	ω_e (cm^{-1})	75				
	T_e (cm^{-1})	24086				
	D_e (cm^{-1})	1717				
$6^2\Sigma^+$	R_e (Å)	3.72				
	ω_e (cm^{-1})	126				
	T_e (cm^{-1})	24164				
	D_e (cm^{-1})	1578				

the low energy side and a broad shoulder to the high energy side. The transition is not vibrationally resolved. The $4^2\Pi$ state correlates to a Ca singlet state, in contrast to the $4^2\Sigma^+$ and $3^2\Pi$ states described above, which both correlate to the same Ca ^{3}D state. This is noteworthy considering the interaction of Ca with He. Calculations have shown that the CaHe potential for the Ca $4s^13d^1,^1$D state has a pronounced minimum for its molecular Π substate, whereas all molecular substates corresponding to Ca $4s^13d^1,^3$D are repulsive or very weakly bound.[66] The lack of vibrational resolution in the $4^2\Pi \leftarrow X^2\Sigma^+$ excitation spectra indicates a stronger interaction of the excited molecule with the droplet surface. The steep rising edge of the peak indicates that the laser excitation starts at the lowest vibrational transition, which is confirmed by our calculations. The onset of the rising edge is shifted to the red by 100 cm^{-1} as compared to the values found in ref 37. Our calculations show that the $4^2\Pi \leftarrow X^2\Sigma^+$ transition has a very high transition dipole moment with a maximum of the Franck−Condon envelope at the 0−0 transition, which could cause an easy saturation of this transition. We have recorded this transition with various laser pulse energies. Although the shoulder on the high energy side does broaden with increasing laser energy, the steep rising edge does not show a significant energy dependence.

An analysis of the atomic signals again shows that Ca follows the LiCa signal; however, at this level of excitation there is a large number of crossings and avoided crossings of molecular potentials that, together with the influence of the He_N environment, increase the possibility of the LiCa molecule being predissociated. The REMPI-TOF signal shows a weak CaHe ion signal that follows the LiCa ion signal in the region of the $4^2\Pi \leftarrow X^2\Sigma^+$ transition (not shown). We explain this in accordance with the detection of fragments in the $3^2\Pi_{1/2,3/2} \leftarrow X^2\Sigma^+$ transition: He droplets could act as an intermediate and lead from an excited LiCa*−He_N system via a LiCa*−He−He_N transition state to the formation of Ca*He exciplexes. Similar exciplex formation processes have been found for Ak−He_N systems.[67,68] The observation that a CaHe ion signal is detected at the $4^2\Pi \leftarrow X^2\Sigma^+$ transition is in agreement with theoretical results in ref 66 wherein a relatively strong binding of the Ca*(^{1}D)He $^1\Pi$ potential was reported.

Two more LiCa transitions have been found, one weak transition between 21250 and 21500 cm^{-1} and a strong transition between 24000 and 25250 cm^{-1}. The assignment of these states to molecular transitions is based on our calculations and will be treated in detail below.

Theoretical Methods and Computational Details. In addition to the experimental investigation we further examine the excited states of LiCa by means of molecular-orbital-based quantum chemistry using the MOLPRO software package.[69] The potential energy curves (PEC) for the lowest 28 states were obtained from multireference configuration interaction (MRCI) calculations[70] based on complete active space self-consistent field (CASSCF) wave functions.[71−74] All calculations were performed in the C_{2v} point group. Orbitals and occupation schemes are referring to the program-specific internal ordering of the irreducible representation ($A_1/B_1/B_2/A_2$). The 10 innermost electrons of the Ca atom were replaced by an effective core potential (ECP) of the Stuttgart group (ECP10MDF).[75] Further improvement, especially of the energy spacing, was obtained by applying a core polarization potential (CPP) with a static dipole polarizability of 3.522 au and a cutoff radius of 1 Å.[76] Because the matching ECP-basis set did not provide enough basis functions for an accurate description of the excited states in the experimentally relevant energy range, we tested several larger all-electron basis sets for compatibility with the ECP. In a series of benchmark calculations on the atomic excitations of Ca we identified the cc-pV5Z basis set[77] as the most suitable compromise between accuracy and computational effort. For Li we chose the aug-cc-pV5Z basis of Peterson.[78] The rather unconventional procedure of combining an all-electron basis set with an ECP was justified by the improved reproducibility of atomic excitations deviating from experimental values by less than 3.5%. Basis functions with angular momentum larger than g had to be removed due to program-internal limitations. The highly relevant d-functions were used in fully uncontracted form. This procedure led to a basis set consisting of (15s9p6d4f3g)/(26s18p8d3f2g) elementary functions and [7s6p6d4f3g] /[8s7p8d3f2g] contracted functions for Ca/Li. The active space consisted of 19 active orbitals (9/4/4/2) filled with three electrons. The 5 lower orbitals were kept doubly occupied in the CASSCF calculation. Of the 28 calculated states, (8/5/5/2) states were calculated in the doublet multiplicity and (3/2/2/1) states in the quartet multiplicity.

Theoretical Results. In Table 3 we compare our curves to previous theoretical results where possible. In general, we find good agreement between the derived spectroscopic parameters. Our calculations tend to slightly overestimate the potential depth, which is a known consequence of the application of effective core potentials.[79] A comparison to experimentally derived molecular parameters is given in Table 4. Good

Table 4. Comparison to Experimentally Determined Molecular Parameters of the Ground and Excited States of LiCa

state	property	calculation	experiment	Russon et al.[37]	Stein et al.[39]
$X^2\Sigma^+$	R_e (Å)	3.342		3.3796(11) (R_0)	3.35582(10)
	ω_e (cm^{-1})	202.6		195.2 ($\Delta G_{1/2}$)	202.2386
	D_e (cm^{-1})	2883		1936	2605.3(100)
$2^2\Sigma^+$	R_e (Å)	3.503			3.48514(3)
	ω_e (cm^{-1})	201.7			202.126(7)
	T_e (cm^{-1})	9461			9572.0483(108)
	D_e (cm^{-1})	8360			7937(10)
$4^2\Sigma^+$	R_e (Å)	3.398		3.3699(37) (R_0)	3.425(1)
	ω_e (cm^{-1})	270	288(7)	284.5 ($\Delta G_{1/2}$)	287.84(2)
	T_e (cm^{-1})	15277	15340(8)	15237.6	15240.07(10)
	D_e (cm^{-1})	8274			7701(10)
$3^2\Pi$	R_e (Å)	3.486		3.5451(36)	
	ω_e (cm^{-1})	152	134(51)	144.5	
	T_e (cm^{-1})	19444	19334(42)	19285.8	
$4^2\Pi$	ω_e (cm^{-1})	179		178.5	
	T_e (cm^{-1})	21980		22257.8	

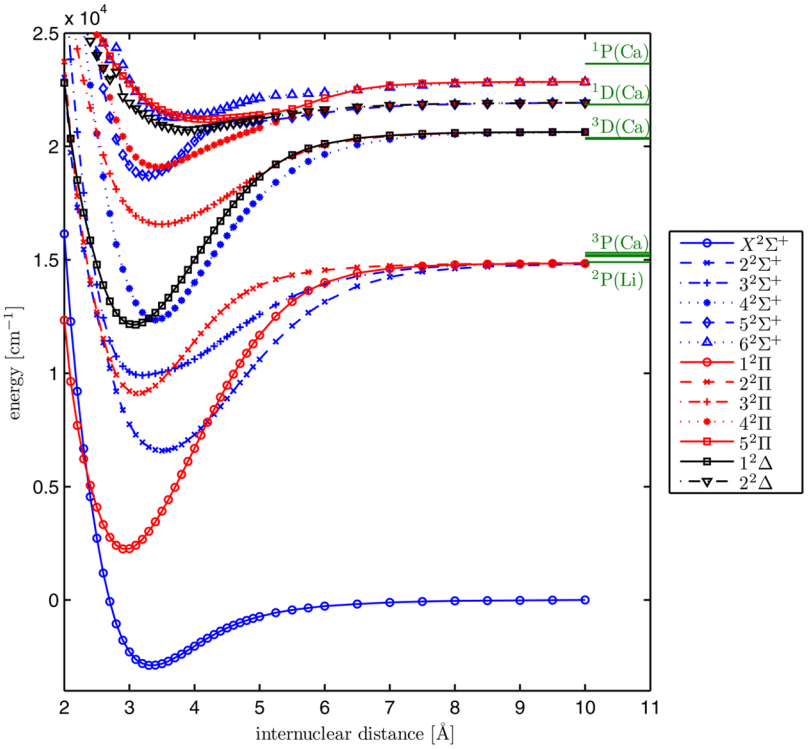

Figure 5. LiCa potential energy curves of the doublet manifold. The calculated asymptotes show a slight deviation from experimental atomic excitation energies (taken from the NIST database[60]).

agreement is found for our results and the theoretical work of Allouche et al.[40] and recent experiments of Stein et al.[39]

Particularly large deviations between different theoretical approaches occur for the X $^2\Sigma^+$ ground state. Single reference approaches tend to predict shorter bond lengths and reduced binding energies. Recently, a potential depth of 2260 cm^{-1} at a distance of 3.395 Å was determined at the coupled cluster level of theory.[16] Kotochigova et al. obtained a potential depth of 2607 cm^{-1} at a distance of 3.364 Å,[17] which is in very good agreement with recent experimental investigations.[39] A comparison to our result for the ground state demonstrates the overestimation of the potential depth. Benchmark calculations using an all electron basis set at the CASSCF/MRCI level with Douglas−Kroll correction of the eighth order yielded a potential depth of 2664 cm^{-1} at a distance of 3.38 Å. A calculation using the ECP gave a potential depth of 3057 cm^{-1} at a distance of 3.36 Å. Inclusion of the CPP finally leads to the improved value listed in Table 3.

Figure 5 contains the PECs of the doublet manifold. For large internuclear distances the $2^2\Sigma^+$ and $3^2\Sigma^+$ states approach nearly the same value, although the atomic excitations show a difference of about 300 cm^{-1}. One asymptotic value lies within 0.6% of the experimentally determined value for the Li $1s^12p,^2P$ excitation[60] and remains independent of minor changes to the basis set and changes to the ECP and CPP. The second asymptotic value shows stronger dependence on ECP and CPP modifications. Previous examinations of this system ran into similar problems.[42] The two states are very close and exhibit an

dx.doi.org/10.1021/jp407818k | J. Phys. Chem. A 2013, 117, 13719−13731

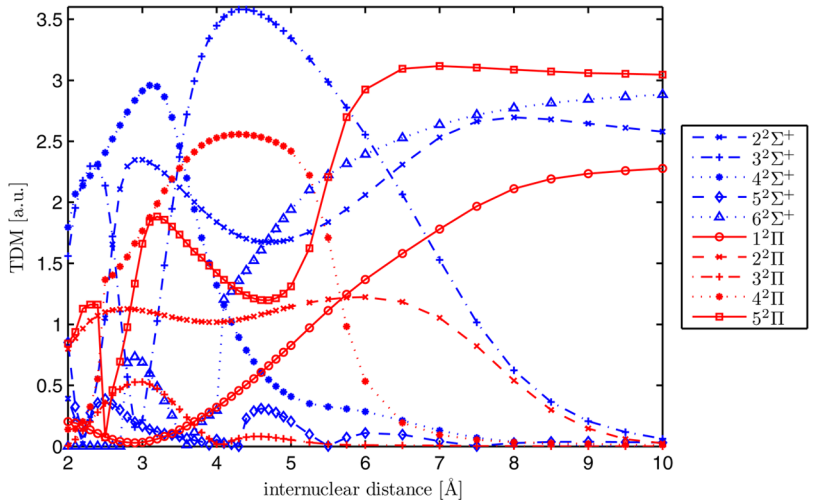

Figure 6. Transition dipole moments for the states shown in Figure 5.

avoided crossing for large internuclear separations. The $1^2\Pi$ and $2^2\Pi$ states show the same behavior for long-range and give the wrong order (Figure 5).

All remaining excited states in Figure 5 converge to atomic excitations of the Ca atom. The states $5^2\Sigma^+$ and $6^2\Sigma^+$ show an avoided crossing at 4.5 Å. Because the energies obtained for large internuclear separation differ from the atomic states,[60] our result for the position (internuclear distance) and energy of the level crossing are not very accurate. The same is valid for the avoided crossing of the states $4^2\Pi$ and $5^2\Pi$ at 5.5 Å. Only after adding an appropriate CPP, the $5^2\Sigma^+$ state shows the strong bonding displayed in Figure 5, without the CPP it appears weakly bound, similar to the $2^2\Delta$ state.

The transition dipole moments (TDMs) for the doublet states are presented in Figure 6. Vertical excitation at the equilibrium distance of the ground state into the $4^2\Sigma^+$ state has the largest transition dipole moment in the given range. This transition gives rise to a strong signal in the experimental measurements. Among the $^2\Pi$ states the $4^2\Pi$ state has the largest TDM for a vertical excitation, which agrees well with the experiment. Transitions into the $2^2\Sigma^+$ and $3^2\Sigma^+$ states have also strong TDMs, but they are outside the range of the experimental investigation. The TDM for the $1^2\Pi$ state is very small, the $2^2\Pi$ state lies outside the range of the experimental investigation. Transitions into the $5^2\Sigma^+$, $6^2\Sigma^+$, $3^2\Pi$, and $5^2\Pi$ states have non-negligible TDMs and are experimentally observed. Dipole transitions from the ground state into to $^2\Delta$ states are forbidden by selection rules and have negligible TDMs.

Figure 7 contains the calculated states of the quartet manifold. Transitions from the $X^2\Sigma^+$ state into quartet states are forbidden and the TDM is zero. The $^4\Sigma^-$ state is strongly bound.

Figures 8 and 9 show the permanent dipole moments of all calculated states. Core polarization effects were neglected, but because there is a good agreement with previous results,[42] the error is expected to be small. For the ground state the permanent dipole moment increases continuously with decreasing internuclear separation until it reaches a value of 0.61 au (1.55 D) at 2.7 Å, and then the value drops. At the equilibrium distance the permanent dipole moment has a value of 0.50 au, only slightly deviating from the value determined by Kotochigova et al. (0.44 au).[17]

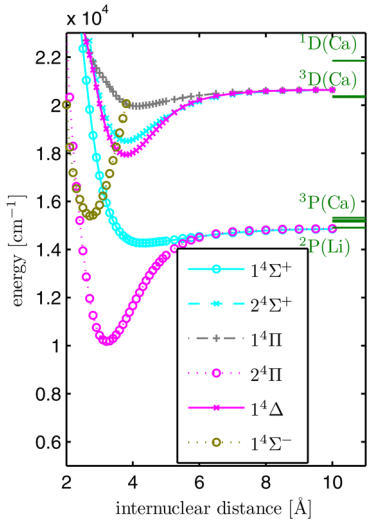

Figure 7. Potential energy curves of the quartet states. Note that the $1^4\Sigma^-$ state was determined only between 2 and 4 Å. The asymptotic values are compared to the NIST values.[60]

Using the computer program betaFit 2.1[80] the PECs of experimentally observed states ($3^2\Pi$, $4^2\Sigma^+$, $4^2\Pi$, $5^2\Sigma^+$, $5^2\Pi$, $6^2\Sigma^+$) were fitted with an analytical function using 11−14 parameters. These potential functions were used in the program LEVEL 8.0[81] to determine the vibronic levels and the Franck−Condon factors. The latter mostly showed strong transitions for the $\nu' = 0$ states with Franck−Condon factors between 0.95 and 0.7. With increasing vibrational quantum number the Franck−Condon factor decreases for these states. Only the $5^2\Pi$ and $6^2\Sigma^+$ states show a maximum of the Franck−Condon factor of about 0.1 at higher vibrational quantum numbers.

Comparison of Theoretical Results to Experimental Results. The calculated PECs and TDMs for the $4^2\Sigma^+ \leftarrow X^2\Sigma^+$ transition confirm our interpretation of the experimental data. We find good agreement between calculated and experimentally determined band origins with deviations below 20 cm^{-1}. The trend of decreasing transition probability with increasing vibrational quantum number ν' is in accordance with the experimental findings.

The theoretically predicted transition energy for the $3^2\Pi_{1/2,3/2} \leftarrow X^2\Sigma^+$ transition is too large: The calculated

dx.doi.org/10.1021/jp407818k | J. Phys. Chem. A 2013, 117, 13719−13731

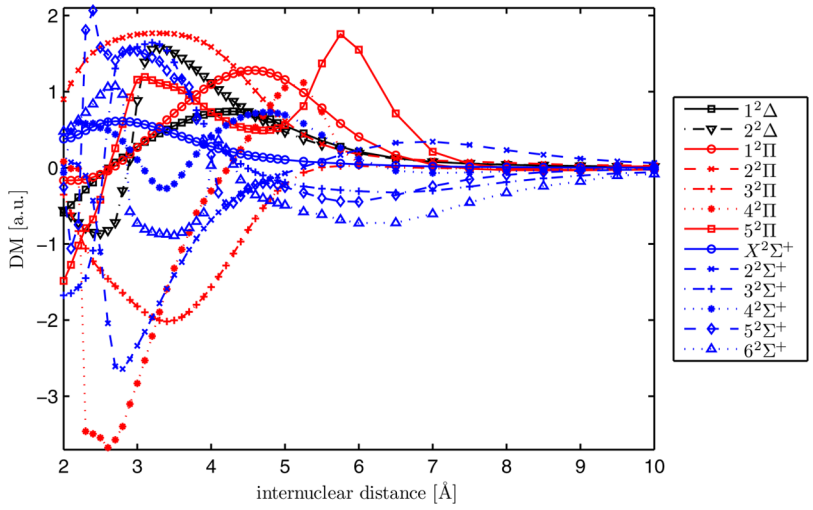

Figure 8. Permanent dipole moments of all doublet states.

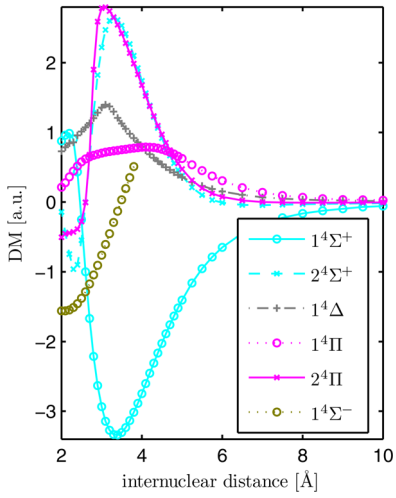

Figure 9. Permanent dipole moments of all quartet states.

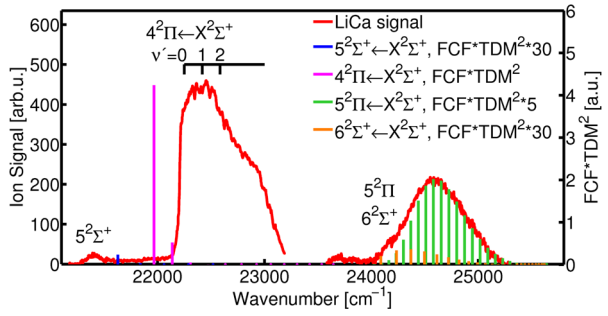

Figure 10. REMPI-TOF signal in the range 21100−25800 cm^{-1}. The red curve shows the smoothed data, the colored vertical lines represent the calculated Franck−Condon factors weighted with the respective transition dipole moments. The FCFs have been scaled to fit to the signal; the scaling factors are given in the legend. The transitions into the $5^2\Sigma^+$, $5^2\Pi$, and $6^2\Sigma^+$ states have not been observed before and are assigned with the help of our calculations. The short black vertical lines above the $4^2\Pi \leftarrow X^2\Sigma^+$ transition refer to values from ref 37. The red vertical line near 22000 cm^{-1} represents our calculated 0−0 band position.

potential energy curve (Figure 5) lies above the atomic value in the separated atom limit. Despite this inaccuracy in the absolute position, the vibrational spacing and the isotope shifts are well reproduced by the calculations.

Figure 10 shows the experimental and the calculated excitation spectra in the range between 21100 and 25500 cm^{-1}. The theoretical spectrum was obtained by multiplying the FCF with the TDM^2 of the respective state at 3.4 Å . The observed bands have been assigned to the $5^2\Sigma^+$, $4^2\Pi$, $6^2\Sigma^+$, and $5^2\Pi$ states, respectively. Although calculations predict an extremely small TDM for the $5^2\Sigma^+ \leftarrow X^2\Sigma^+$ transition, a weak signal originating from this transition is experimentally observed. This state did not occur in previous experiments. Its transition probability might be enhanced by interactions with the helium environment. The theoretically predicted values are at slightly higher energies than the experimental values. The next structure in the spectra could clearly be associated with the $4^2\Pi$ state. This state was also investigated experimentally by Russon et al.,[37] but due to the interaction with the droplet, the vibrational states could not be resolved in the experiment. For the $4^2\Pi$ state the interaction between the helium and the diatomic molecule is relatively strong, which is indicated by the deep potential between a Ca atom in this excited state and a He atom, as can be seen in the diatomic potential curves in ref 66.

The deviation between the theoretical and experimental line positions can be explained by taking a look at Figure 5. The two highest $^2\Pi$ states show an avoided crossing, which means that the $4^2\Pi$ state is associated with the ^{1}P Ca atomic limit. The potential at large internuclear separation is about 300 cm^{-1} below the atomic value,[60] which corresponds to the difference between the theoretical and experimental values for the $4^2\Pi \leftarrow X^2\Sigma^+$ transition. On the basis of our calculations, we can assign the structure between 24000 and 25000 cm^{-1} to the $6^2\Sigma^+$ and $5^2\Pi$ states. The calculated Franck−Condon factors are in excellent agreement with the experimentally observed structure and the deviation of the position is less than 100 cm^{-1}. This good correspondence is probably related to the good reproduction of less than 100 cm^{-1} of the atomic ^{1}D (Ca) state at large internuclear separations. Because of an avoided crossing the functions that describe the $5^2\Pi$ state at large internuclear separations are the same that describe the $4^2\Pi$ state at small internuclear distances. The calculated asymptotic value (^{1}P Ca state) obtained for the $5^2\Pi$ state deviates from the exact value. Because of the avoided crossing, we expect that the $4^2\Pi$ potential energy curve shows a similar deviation at small internuclear separations. The main features of this transition

dx.doi.org/10.1021/jp407818k | J. Phys. Chem. A 2013, 117, 13719−13731

can be explained by the $5^2\Pi$ state, which has a strong transition dipole moment. The vibrational states of this transition are not resolved because of the narrow vibrational spacing of ω_e = 75 cm^{-1}. The rising edge deviates from the prediction, which can be explained by the additional contribution of the $6^2\Sigma^+$ state to the signal. For this structure a significant Li ion-signal was obtained, in contrast to the behavior of all other recorded transitions. This can be explained by the interaction with even higher states. For the limit of separated atoms the states Li $3s^1,^2S$ + Ca $4s^2,^1S$ and Li $2p^1,^2P$ + Ca $4s^14p^1,^3P$ would follow, both including an excited Li atom. The PECs of states converging to excited Li approach the $6^2\Sigma^+$ and $5^2\Pi$ states and for the $6^2\Sigma^+$ state an avoided crossing is indicated by the potential form and a discontinuity in the transition dipole moment (Figures 5 and 6).

CONCLUSION

We have presented a comprehensive experimental and theoretical study of the LiCa molecule. We show that these molecules can be formed very efficiently on helium nanodroplets by using a sequential pickup scheme. Our results represent the first experimental observation of mixed alkali−alkaline earth molecules on helium nanodroplets. A comparison of our experimental results for the $X^2\Sigma^+$, $4^2\Sigma^+$, $3^2\Pi$, and $4^2\Pi$ states with those of previous molecular beam[37] and recent heat-pipe oven[38,39] experiments reveal that the determined molecular parameters of LiCa on He_N lie within a few cm^{-1} of the gas phase values. This demonstrates the capability of helium droplet isolation spectroscopy for the characterization of alkali−alkaline earth molecules. The interaction between droplet and molecule manifests itself in the appearance of phonon wings in the spectra. They are caused by the coupling of the vibrational motion of the LiCa molecule to excitation modes of the helium droplet and extend from the vibronic band origin toward higher energies. For the $4^2\Sigma^+$ and $3^2\Pi$ states the vibrational spacing in combination with narrow phonon wings allows the separation of vibrational states. The narrow, lambda-shaped peak form, which is typical for surface bound molecules,[28] indicates a surface location of LiCa.

Ab initio quantum chemical calculations of potential energy curves, transition dipole moments, Franck−Condon factors, and permanent dipole moments support our spectroscopic study of the LiCa molecule. The 19 lowest lying potential energy curves were determined by using a multireference configuration interaction calculation. On the basis of our calculations, we were able to identify the previously unobserved transitions into the $5^2\Sigma^+$, $5^2\Pi$, and $6^2\Sigma^+$ states. Our results for the lower excited states and the ground state of LiCa agree well with previous calculations[16−18,40−42] and extend the previous works on LiCa to higher excited states. Despite the perturbation of the molecule by the droplet, the resolution of the experimental spectra obtained for LiCa is sufficient to test calculated potential energy curves. LiCa has been taken as an alkali−alkaline earth prototype molecule because of the available experimental and theoretical reference data. The experimental results serve as a proof of principle and demonstrate that formation of alkali−alkaline earth molecules on helium nanodroplets is possible. Our results indicate that the preparation of various tailor-made alkali−alkaline earth molecules on helium droplet will be possible, opening a new route for the characterization of these molecules. This could be an important contribution for the preparation of ultracold molecules from ultracold atoms, a process which relies on the knowledge of accurate potential energy curves. We think that the most promising candidate for the production of ultracold Ak−Ake ground state molecules is the RbSr molecule.[19] Both Rb and Sr atoms are surface bound species and have been well characterized on helium droplets. On the basis of our results for LiCa, we conclude that the formation of RbSr molecules for the determination of molecular parameter is feasible. Beyond the scope of this article, our results suggest that the molecules which desorb upon excitation can be further investigated with additional lasers, which would overcome resolution constraints and lead to ro-vibrationally resolved spectra.

AUTHOR INFORMATION

Corresponding Authors

*F. Lackner: e-mail, florian.lackner@tugraz.at.
*W. E. Ernst: e-mail, wolfgang.ernst@tugraz.at.

Notes

The authors declare no competing financial interest.

ACKNOWLEDGMENTS

We thank Andreas W. Hauser for stimulating and helpful discussions. This research has been supported by the Austrian Science Fund (FWF) under Grant FWF-E-P19759 and the ERDF Program of the European Union and the Region of Styria.

REFERENCES

(1) Quemener, G.; Julienne, P. S. Ultracold Molecules under Control! *Chem. Rev.* **2012**, *112*, 4949−5011.
(2) Micheli, A.; Brennen, G.; Zoller, P. A Toolbox for Lattice-Spin Models with Polar Molecules. *Nat. Phys.* **2006**, *2*, 341−347.
(3) Pupillo, G.; Griessner, A.; Micheli, A.; Ortner, M.; Wang, D.-W.; Zoller, P. Cold Atoms and Molecules in Self-Assembled Dipolar Lattices. *Phys. Rev. Lett.* **2008**, *100*, 050402.
(4) Kajita, M.; Gopakumar, G.; Abe, M.; Hada, M. Elimination of the Stark Shift from the Vibrational Transition Frequency of Optically Trapped $^{174}Yb^6Li$ Molecules. *Phys. Rev. A* **2011**, *84*, 022507.
(5) Kajita, M.; Gopakumar, G.; Abe, M.; Hada, M. Sensitivity of Vibrational Spectroscopy of Optically Trapped SrLi and CaLi Molecules to Variations in mp/me. *J. Phys. B: At. Mol. Opt.* **2013**, *46*, 025001.
(6) Ospelkaus, S.; Ni, K.-K.; Wang, D.; de Miranda, M. H. G.; Neyenhuis, B.; Quéméner, G.; Julienne, P. S.; Bohn, J. L.; Jin, D. S.; Ye, J. Quantum-State Controlled Chemical Reactions of Ultracold Potassium-Rubidium Molecules. *Science* **2010**, *327*, 853−857.
(7) Brue, D. A.; Hutson, J. M. Prospects of Forming Ultracold Molecules in $^2\Sigma$ States by Magnetoassociation of Alkali-Metal Atoms with Yb. *Phys. Rev. A* **2013**, *87*, 052709.
(8) Hansen, A. H.; Khramov, A.; Dowd, W. H.; Jamison, A. O.; Ivanov, V. V.; Gupta, S. Quantum Degenerate Mixture of Ytterbium and Lithium Atoms. *Phys. Rev. A* **2011**, *84*, 011606.
(9) Ivanov, V. V.; Khramov, A.; Hansen, A. H.; Dowd, W. H.; Münchow, F.; Jamison, A. O.; Gupta, S. Sympathetic Cooling in an Optically Trapped Mixture of Alkali and Spin-Singlet Atoms. *Phys. Rev. Lett.* **2011**, *106*, 153201.
(10) Munchow, F.; Bruni, C.; Madalinski, M.; Gorlitz, A. Two-photon Photoassociation Spectroscopy of Heteronuclear YbRb. *Phys. Chem. Chem. Phys.* **2011**, *13*, 18734−18737.
(11) Kraft, S.; Vogt, F.; Appel, O.; Riehle, F.; Sterr, U. Bose-Einstein Condensation of Alkaline Earth Atoms: ^{40}Ca. *Phys. Rev. Lett.* **2009**, *103*, 130401.
(12) Stellmer, S.; Tey, M. K.; Huang, B.; Grimm, R.; Schreck, F. Bose-Einstein Condensation of Strontium. *Phys. Rev. Lett.* **2009**, *103*, 200401.

(13) de Escobar, Y. N. M.; Mickelson, P. G.; Yan, M.; DeSalvo, B. J.; Nagel, S. B.; Killian, T. C. Bose-Einstein Condensation of ^{84}Sr. *Phys. Rev. Lett.* **2009**, *103*, 200402.
(14) Stellmer, S.; Grimm, R.; Schreck, F. Production of Quantum-Degenerate Strontium Gases. *Phys. Rev. A* **2013**, *87*, 013611.
(15) Zuchowski, P. S.; Aldegunde, J.; Hutson, J. M. Ultracold RbSr Molecules Can Be Formed by Magnetoassociation. *Phys. Rev. Lett.* **2010**, *105*, 153201.
(16) Gopakumar, G.; Abe, M.; Kajita, M.; Hada, M. ab initio Study of Permanent Electric Dipole Moment and Radiative Lifetimes of Alkaline-Earth-Metal-Li Molecules. *Phys. Rev. A* **2011**, *84*, 062514.
(17) Kotochigova, S.; Petrov, A.; Linnik, M.; Klos, J.; Julienne, P. S. Ab Initio Properties of Li-Group-II Molecules for Ultracold Matter Studies. *J. Chem. Phys.* **2011**, *135*, 164108.
(18) Augustovičová, L.; Soldán, P. Ab Initio Properties of MgAlk (Alk = Li, Na, K, Rb, Cs). *J. Chem. Phys.* **2012**, *136*, 084311.
(19) Pasquiou, B.; Bayerle, A.; Tzanova, S.; Stellmer, S.; Szczepkowski, J.; Parigger, M.; Grimm, R.; Schreck, F. Quantum Degenerate Mixtures of Strontium and Rubidium Atoms. *arXiv preprint arXiv:1305.5935* 2013.
(20) Ulmanis, J.; Deiglmayr, J.; Repp, M.; Wester, R.; Weidemüller, M. Ultracold Molecules Formed by Photoassociation: Heteronuclear Dimers, Inelastic Collisions, and Interactions with Ultrashort Laser Pulses. *Chem. Rev.* **2012**, *112*, 4890−4927.
(21) Köhler, T.; Góral, K.; Julienne, P. S. Production of Cold Molecules via Magnetically Tunable Feshbach Resonances. *Rev. Mod. Phys.* **2006**, *78*, 1311−1361.
(22) Danzl, J. G.; Mark, M. J.; Haller, E.; Gustavsson, M.; Hart, R.; Aldegunde, J.; Hutson, J. M.; Nägerl, H.-C. An Ultracold High-Density Sample of Rovibronic Ground-State Molecules in an Optical Lattice. *Nat. Phys.* **2010**, *6*, 265−270.
(23) Danzl, J. G.; Haller, E.; Gustavsson, M.; Mark, M. J.; Hart, R.; Bouloufa, N.; Dulieu, O.; Ritsch, H.; Nägerl, H.-C. Quantum Gas of Deeply Bound Ground State Molecules. *Science* **2008**, *321*, 1062−1066.
(24) Ni, K.-K.; Ospelkaus, S.; De Miranda, M.; Pe'er, A.; Neyenhuis, B.; Zirbel, J.; Kotochigova, S.; Julienne, P.; Jin, D.; Ye, J. A High Phase-Space-Density Gas of Polar Molecules. *Science* **2008**, *322*, 231−235.
(25) Stellmer, S.; Pasquiou, B.; Grimm, R.; Schreck, F. Creation of Ultracold Sr_2 Molecules in the Electronic Ground State. *Phys. Rev. Lett.* **2012**, *109*, 115302.
(26) Callegari, C.; Ernst, W. E. Helium Droplets as Nanocryostats for Molecular Spectroscopy - from the Vacuum Ultraviolet to the Microwave Regime. In *Handbook of High-Resolution Spectroscopy*; Quack, M., Merkt, F., Eds.; John Wiley & Sons: Chichester, U.K., 2011; pp 1551−1594.
(27) Allard, O.; Nagl, J.; Auböck, G.; Callegari, C.; Ernst, W. E. Investigation of KRb and Rb_2 Formed on Cold Helium Nanodroplets. *J. Phys. Chem. B* **2006**, *39*, 1169.
(28) Higgins, J.; Callegari, C.; Reho, J.; Stienkemeier, F.; Ernst, W. E.; Gutowski, M.; Scoles, G. Helium Cluster Isolation Spectroscopy of Alkali Dimers in the Triplet Manifold. *J. Chem. Phys. A* **1998**, *102*, 4952−4965.
(29) Mudrich, M.; Bünermann, O.; Stienkemeier, F.; Dulieu, O.; Weidemüller, M. Formation of Cold Bialkali Dimers on Helium Nanodroplets. *Eur. Phys. J. D* **2004**, *31*, 291−299.
(30) Auböck, G.; Nagl, J.; Callegari, C.; Ernst, W. E. Triplet State Excitation of Alkali Molecules on Helium Droplets: Experiments and Theory. *J. Phys. Chem. A* **2007**, *111*, 7404−7410.
(31) Nagl, J.; Aubëk, G.; Hauser, A. W.; Allard, O.; Callegari, C.; Ernst, W. E. High-Spin Alkali Trimers on Helium Nanodroplets: Spectral Separation and Analysis. *J. Chem. Phys.* **2008**, *128*, 154320.
(32) Nagl, J.; Auböck, G.; Hauser, A. W.; Allard, O.; Callegari, W. E. C.and Ernst Heteronuclear and Homonuclear High-Spin Alkali Trimers on Helium Nanodroplets. *Phys. Rev. Lett.* **2008**, *100*, 063001.
(33) Hauser, A. W.; Ernst, W. E. Homo- and Heteronuclear Alkali Metal Trimers Formed on Helium Nanodroplets. Part I. Vibronic Spectra Simulations Based on Ab Initio Calculations. *Phys. Chem. Chem. Phys.* **2011**, *13*, 18762−18768.
(34) Giese, C.; Stienkemeier, F.; Mudrich, M.; Hauser, A. W.; Ernst, W. E. Homo- and Heteronuclear Alkali Metal Trimers Formed on Helium Nanodroplets. Part II. Femtosecond Spectroscopy and Spectra Assignments. *Phys. Chem. Chem. Phys.* **2011**, *13*, 18769−18780.
(35) Lackner, F.; Poms, J.; Krois, G.; Pototschnig, J. V.; Ernst, W. E. Spectroscopy of Lithium Atoms and Molecules on Helium Nanodroplets. *J. Phys. Chem. A* **2013**, DOI: 10.1021/jp4030238.
(36) Hizhnyakov, V.; Tehver, I.; Benedek, G. Theory of the Optical Spectrum of Na_2 on ^{4}He Droplets: Effects of the Zero-Point Energy of the Nearest Atoms. *Eur. Phys. J. B* **2009**, *70*, 507−512.
(37) Russon, L. M.; Rothschopf, G. K.; Morse, M. D.; Boldyrev, A. I.; Simons, J. Two-Photon Ionization Spectroscopy and All-Alectron Ab Initio Study of LiCa. *J. Chem. Phys.* **1998**, *109*, 6655−6665.
(38) Ivanova, M.; Stein, A.; Pashov, A.; Stolyarov, A. V.; Knockel, H.; Tiemann, E. The $X^2\Sigma^+$ State of LiCa Studied by Fourier-Transform Spectroscopy. *J. Chem. Phys.* **2011**, *135*, 174303.
(39) Stein, A.; Ivanova, M.; Pashov, A.; Knöckel, H.; Tiemann, E. Spectroscopic Study of the $2^2\Sigma^+$ and the $4^2\Sigma^+$ Excited States of LiCa. *J. Chem. Phys.* **2013**, *138*, 114306.
(40) Allouche, A.; Aubert-Frécon, M. Theoretical Study of Low-lying Electronic States of the CaLi Molecule. *Chem. Phys. Lett.* **1994**, *222*, 524−528.
(41) Guérout, R.; Aymar, M.; Dulieu, O. Ground State of the Polar Alkali-Metal-Atom-Strontium Molecules: Potential Energy Curve and Permanent Dipole Moment. *Phys. Rev. A* **2010**, *82*, 042508.
(42) Gopakumar, G.; Abe, M.; Hada, M.; Kajita, M. Ab Initio Study of Ground and Excited States of ^{6}Li^{40}Ca and ^{6}Li^{88}Sr Molecules. *J. Chem. Phys.* **2013**, *138*, 194307−14.
(43) Vergés, J.; D'Incan, J.; Effantin, C.; Bernard, A.; Fabre, G.; Stringat, R.; Boulezhar, A. Electronic structure of BaLi: The $(2)^2\Sigma^+$ State. *J. Phys. B: At. Mol. Opt.* **1994**, *27*, L153.
(44) D'Incan, J.; Effantin, C.; Bernard, A.; Fabre, G.; Stringat, R.; Boulezhar, A.; Vergés, J. Electronic Structure of BaLi. II. First Observation of the Ba^{6,7}Li Spectrum: Analysis of the $(2)^2\Pi \rightarrow X^2\Sigma^+$ System. *J. Chem. Phys.* **1994**, *100*, 945−949.
(45) Stringat, R.; Fabre, G.; Boulezhar, A.; Dincan, J.; Effantin, C.; Verges, J.; Bernard, A. The $X^2\Sigma^+$, $(2)^2\Sigma^+$, and $(2)^2\Pi$ States of BaLi. *J. Mol. Spectrosc.* **1994**, *168*, 514−521.
(46) Nagl, J.; Hauser, A. W.; Auböck, G.; Callegari, C.; Ernst, W. E. Optical Spectroscopy of Potassium-Doped Argon Clusters. Experiments and Quantum-Chemistry Calculations. *J. Phys. Chem. A* **2007**, *111*, 12386−12397.
(47) Lackner, F.; Krois, G.; Theisen, M.; Koch, M.; Ernst, W. E. Spectroscopy of *n*S, *n*P, and *n*D Rydberg Series of Cs Atoms on Helium Nanodroplets. *Phys. Chem. Chem. Phys.* **2011**, *13*, 18781−18788.
(48) Lewerenz, M.; Schilling, B.; Toennies, J. A New Scattering Deflection Method for Determining and Selecting the Sizes of Large Liquid Clusters of ^{4}He. *Chem. Phys. Lett.* **1993**, *206*, 381−387.
(49) Toennies, J. P.; Vilesov, A. F. Superfluid Helium Droplets: A Uniquely Cold Nanomatrix for Molecules and Molecular Complexes. *Angew. Chem., Int. Ed.* **2004**, *43*, 2622−2648.
(50) Scheidemann, A. A.; Kresin, V. V.; Hess, H. Capture of Lithium by ^{4}He Clusters: Surface Adsorption, Penning Ionization, and Formation of $HeLi^+$. *J. Chem. Phys.* **1997**, *107*, 2839−2844.
(51) Stienkemeier, F.; Meier, F.; Lutz, H. Alkaline Earth Metals (Ca, Sr) Attached to Liquid Helium Droplets: Inside or out. *J. Chem. Phys.* **1997**, *107*, 10816.
(52) Ren, Y.; Kresin, V. V. Surface Location of Alkaline-Earth-Metal-Atom Impurities on Helium Nanodroplets. *Phys. Rev. A* **2007**, *76*, 043204.
(53) Jones, K. M.; Maleki, S.; Bize, S.; Lett, P. D.; Williams, C. J.; Richling, H.; Knöckel, H.; Tiemann, E.; Wang, H.; Gould, P. L.; Stwalley, W. C. Direct Measurement of the Ground-State Dissociation Energy of Na_2. *Phys. Rev. A* **1996**, *54*, R1006−R1009.
(54) Hizhnyakov, V.; Benedek, G. Vibronic Transitions Between States with Hard and Soft Phonon Dynamics. *Chem. Phys. Lett.* **2008**, *460*, 447−450.

(55) Tehver, I.; Hizhnyakov, V.; Benedek, G. Sodium Molecule on the Surface of Liquid Helium-4 droplets: Optical Transitions Probe Collective Excitations. *Phys. Status Solidi C* **2013**, *10*, 232−235.
(56) Stienkemeier, F.; Higgins, J.; Ernst, W.; Scoles, G. Spectroscopy of Alkali Atoms and Molecules Attached to Liquid He Clusters. *Z. Phys. B* **1995**, *98*, 413−416.
(57) Auböck, G.; Nagl, J.; Callegari, C.; Ernst, W. E. Observation of Relativistic E x e Vibronic Coupling in Rb_3 and K_3 Quartet States on Helium Droplets. *J. Chem. Phys.* **2008**, *129*, 114501.
(58) Herzberg, G. *Molecular Spectra and Molecular Structure I. Spectra of Diatomic Moleules*; Van Nostrand Reinhold: New York, 1950.
(59) Brühl, F. R.; Miron, R. A.; Ernst, W. E. Triplet states of rubidium dimers on helium nanodroplets. *J. Chem. Phys.* **2001**, *115*, 10275−10281.
(60) Ralchenko, Y.; Kramida, A.; Reader, J. *N. A. T. NIST Atomic Spectra Database* (ver. 4.1.0); National Institute of Standards and Technology, Gaithersburg, MD, 2011,
(61) Lefebvre-Brion, H.; Field, R. *The Spectra and Dynamics of Diatomic Molecules*; Elsevier: Amsterdam, 2004.
(62) Mulliken, R. S. Some Neglected Subcases of Predissociation in Diatomic Molecules. *J. Chem. Phys.* **1960**, *33*, 247−252.
(63) Higgins, J.; Callegari, C.; Reho, J.; Stienkemeier, F.; Ernst, W. E.; Lehmann, K. K.; Gutowski, M.; Scoles, G. Photoinduced Chemical Dynamics of High-Spin Alkali Trimers. *Science* **1996**, *273*, 629−631.
(64) Loginov, E.; Drabbels, M. Excited State Dynamics of Ag Atoms in Helium Nanodroplets. *J. Phys. Chem. A* **2007**, *111*, 7504−7515.
(65) Kautsch, A.; Koch, M.; Ernst, W. E. Electronic Relaxation after Resonant Laser Excitation of Cr in Superfluid Helium Nanodroplets. *J. Phys. Chem. A* **2013**, DOI: 10.1021/jp312336m.
(66) Czuchaj, E.; Krosnicki, M.; Stoll, H. Valence Ab Initio Calculation of the Potential Energy Curves for Ca-Rare Gas Van Der Waals Molecules. *Chem. Phys.* **2003**, *292*, 101−110.
(67) Stienkemeier, F.; Higgins, J.; Callegari, C.; Kanorsky, S. I.; Ernst, W. E.; Scoles, G. Spectroscopy of Alkali Atoms (Li, Na, K) Attached to Large Helium Clusters. *Z. Phys. D: At., Mol. Clusters* **1996**, *38*, 253−263.
(68) Reho, J.; Callegari, C.; Higgins, J.; Ernst, W. E.; Lehmann, K. K.; Scolesw, G. Spin-orbit effects in the formation of the Na-He excimer on the surface of He clusters. *Faraday Discuss.* **1997**, *108*, 161−174.
(69) Werner, H.-J.; Knowles, P. J.; Knizia, G.; Manby, F. R.; Schütz, M.; Celani, P.; Korona, T.; Lindh, R.; Mitrushenkov, A.; Rauhut, G.; et al. *MOLPRO, A Package of Ab Initio Programs*, Version 2010.1, 2010; see http://www.molpro.net/.
(70) Knowles, P. J.; Werner, H.-J. Internally Contracted Multi-configuration Reference Configuration Interaction Calculations for Excited States. *Theor. Chim. Acta* **1992**, *84*, 95−103.
(71) Werner, H. J.; Meyer, W. A Quadratically Convergent Multiconfiguration-self-consistent Field Method With Simultaneous-optimization of Orbitals and Cl Coefficients. *J. Chem. Phys.* **1980**, *73*, 2342−2356.
(72) Werner, H.-J.; Meyer, W. A Quadratically Convergent MCSCF Method for the Simultaneous Optimization of Several States. *J. Chem. Phys.* **1981**, *74*, 5794−5801.
(73) Werner, H.-J.; Knowles, P. J. A Second Order MCSCF Method with Optimum Convergence. *J. Chem. Phys.* **1985**, *82*, 5053.
(74) Knowles, P. J.; Werner, H.-J. An Efficient Second Order MCSCF Method for Long Configuration Expansions. *Chem. Phys. Lett.* **1985**, *115*, 259−267.
(75) Lim, I. S.; Stoll, H.; Schwerdtfeger, P. Relativistic Small-Core Energy-Consistent Pseudopotentials for the Alkaline-Earth Elements from Ca to Ra. *J. Chem. Phys.* **2006**, *124*, 034107.
(76) Aymar, M.; Dulieu, O. The Electronic Structure of the Alkaline-Earth-Atom (Ca, Sr, Ba) Hydride Molecular Ions. *J. Phys. B: At. Mol. Opt.* **2012**, *45*, 215103.
(77) Koput, J.; Peterson, K. A. Ab Initio Potential Energy Surface and Vibrational-Rotational Energy Levels of $X^2\Sigma^+$ CaOH. *J. Phys. Chem. A* **2002**, *106*, 9595−9599.
(78) Prascher, B. P.; Woon, D. E.; Peterson, K. A.; Dunning, T. H.; Wilson, A. K. Gaussian Basis Sets for Use in Correlated Molecular Calculations. VII. Valence, Core-Valence, and Scalar Relativistic Basis Sets for Li, Be, Na, and Mg. *Theor. Chem. Acc.* **2011**, *128*, 69−82.
(79) Konowalow, D. D.; Regan, R. M.; Rosenkrantz, M. E. The "Most Likely" Potential Energy Curve for the Lowest $^3\Sigma_u^+$ State of Li_2. *J. Chem. Phys.* **1984**, *81*, 4534−4536.
(80) Le Roy, R. J. *BetaFit 2.1*; University of Waterloo Chemical Physics Research Report CP-666, 2013; A Computer Program to Fit Pointwise Potentials to Selected Analytic Functions.
(81) Le Roy, R. J. *Level 8.0*; University of Waterloo Chemical Physics Research Report CP-663, 2007; A Computer Program for Solving the Radial Schrödinger Equation for Bound and Quasibound Levels.